RSC Advances

ROYAL SOCIETY OF CHEMISTRY

www.rsc.org/advances

Efficient blue fluorescent organic light-emittingdiodes based on novel 9,10-diphenyl-anthracene derivatives

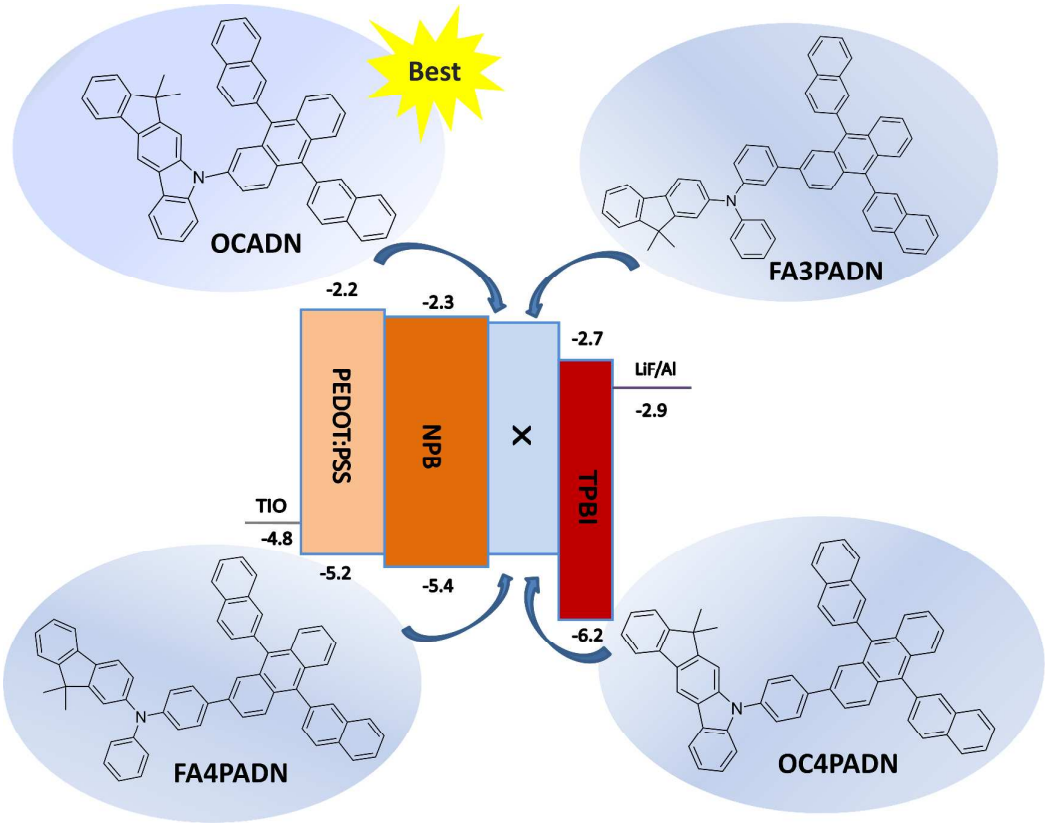

Five 9,10-di(naphthalen-2-yl)anthracene (**ADN**) derivatives with fluorenamine or indenocarbazole moiety have been successfully developed for blue emitters of OLEDs. All materials showed good chemical and thermal stability, moreover the **OCADN** based device exhibited highly efficient sky-blue emission with current efficiency of 2.25 cd/A, power efficiency of 1.13 lm/W and CIE(x,y) coordinate of (0.16, 0.30) at 8 V.

RSC Advances

RSCPublishing

PAPER

Efficient blue fluorescent organic light-emitting diodes based on novel 9,10-diphenyl-anthracene derivatives

Cite this: DOI: 10.1039/x0xx00000x

Received 00th January 2012,
Accepted 00th January 2012

DOI: 10.1039/x0xx00000x

www.rsc.org/

Hongwei Chen, [+a] Wenqing Liang, [+b] Yi Chen, [a] Guojian Tian, [a] Qingchen Dong, *[b] Jinhai Huang, * [a] and Jianhua Su [a]

A series of novel 9,10-di(naphthalen-2-yl) anthracene (ADN) derivatives were designed and synthesized as blue fluorescent emissive materials by inducing diverse aromatic groups to C-2 position of ADN. UV-Vis absorption, fluorescence emission spectroscopy and cyclic voltammetry (CV) were carried out to generally investigate the relationships between the physical properties and molecular structures. Moreover, four non-doped OLED devices adopting **OCADN**, **FA3PADN**, **FA4PADN** and **OC4PADN** as emitting materials were fabricated to study their electroluminescence (EL) performances. Among them, device based on **OCADN** exhibited highly efficient sky-blue emission with current efficiency of 2.25 cd/A, power efficiency of 1.13 lm/W and $CIE_{(x,y)}$ coordinate of (0.16, 0.30) at 8 V. In addition, the device of **OC4PADN** showed efficient blue emission with $CIE_{(x,y)}$ coordinate of (0.16, 0.14) at 8 V.

Introduction

Organic light-emitting diodes (OLEDs) have attracted enormous attentions owing to their excellent performances such as rapid response, high brightness, flexibility, low driving voltage and full-color emission, etc.[1-5] Because of its high technological potential for high-quality flat-panel displays and solid state lighting, OLEDs have made great process and successfully applied in mobile phones and digital cameras since Tang and his co-workers firstly introduced an efficient OLEDs.[6-9] To achieve full-color displays, the red, green and blue emission of relatively equal stability, efficiency and color purity were required. Although a great number of red and green emitters have been developed to satisfy the requirements of OLEDs in the practical usage, efficient and stable organic blue emitting materials are still rare.[10-14] Thus, the development of blue-emitting materials with high performance still remains to be challenge.

To date, many small-molecule emitters, including anthracene[10-18], carbazole[19-22], fluorine[23-25], triarylamine[26-28], and pyrene[29-31] derivatives, have been reported for application in blue OLEDs. As known to all, anthracene was widely used as an attractive building block and starting material for fluorescent blue emitting in OLEDs, due to its high fluorescence quantum yield, wide energy band-gap and easy modification.[1,10-18] However, the anthracene with large π-conjugation is easy to aggregate in condensed phase, leading to fluorescence quenching and emission wavelength red-shift. Thus, many endeavours have been made to avoid the planar configuration by introducing different functionalized blocks to the 9,10-positions of anthracene.[1,32-38] For example, Shi and Tang firstly reported a 9,10-substitued ahthracene derivatives, the di(2-naphthyl) anthracene (ADN), as blue emitter host in 2002. [39] But the incorporation of two perpendicular naphthyl can not completely overcome the red-shifting and fluorescence quenching problems. Therefore, some further work has been processed about introducing different bulky groups at 2,3,6,7-positions of ADN, and their devices showed good morphologic stability and performance, indicating that the molecule

[a] Key Laboratory for Advanced Materials and Institute of Fine Chemicals, East China University of Science & Technology, Shanghai 200237, P. R. China. Fax:（86）21-64252288；Tel:（86）21-64252288；E-mail: huangjh@eucst.edu.cn

[b] MOE Key Laboratory for Interface Science and Engineering in Advanced Materials and Research Center of Advanced Materials Science and Technology, Taiyuan University of Technology, 79 Yingze West Street, Taiyuan 030024, P.R. China. E-mail: donggingchen@tyut.edu.cn

[+] These two authors contribute equally to this work

† Electronic Supplementary Information (ESI) available: See DOI: 10.1039/b000000x/

aggression can be remarkably suppressed by disrupting the symmetry of ADN.[40-43]

Fluorene derivatives were also widely used in OLEDs as blue emitter due to several advantages including their capability of emitting in the blue region spectrum, chemical and morphologic stability, and thermal durability under operation.[23-25] Arylamine group is well-known for its ability to transport charge carriers, and incorporated it into other molecules can improve hole injection and carrier transport properties and increase bulky volumes and thermal stability, as well as improve device stability due to the amorphous structure, charge balance and reduce energy consumption.[26-28] And the materials with fluorenamine or indenocarbazole group have shown excellent hole-injection and transporting capability.[28,43-45]

With respect to all mentioned above, in this work, five asymmetric blue light emitting materials of the ADN derivatives, N-(9,9-dimethyl-9H-fluoren-2-yl)-9,10-di(naphthalen-2-yl)-N-phenyl-anthracen-2-amine (**FAADN**), 5-(9,10-di(naphthalen-2-yl)anthracen-2-yl)-7,7-dimethyl-5,7-dihydro-indenocarbazole (**OCADN**), N-(3-(9,10-di(naphthalen-2-yl) anthracen-2-yl)phenyl)-9,9-dimethyl-N-phenyl-9H-fluoren-2-amine (**FA3PADN**), 9,9-dimethyl-N-phenyl-N-(4-(4,4,5,5-tetramethyl-1,3,2-dioxaborolan-2-yl)phenyl)-9H-fluoren-2-amine (**FA4PADN**) and 7,7-dimethyl-5-(4-(4,4,5,5-tetramethyl-1,3,2-dioxaborolan-2-yl)phenyl)-5,7-dihydroindeno carbazole (**OC4PADN**) were designed and synthesized. The fluorenamine and indenocarbazole moiety which were introduced to the 2-position of di(2-naphthyl) anthracene were to prevent the emission red-shifting and fluorescence quenching in solid, as well as to increase the hole transporting capability, thermal stability and morphologic stability. The incorporation of a phenyl bridge between ADN core and modified moiety is aimed to increase the molecule twisty degree of the molecule and reduce the π-electron conjugation between the two moieties. In order to explore the influence of these substituents of ADN, we fully investigated the thermal and photophysical properties and measured the HOMO and LUMO values. Moreover, to estimate the practical utilities of these ADN derivatives, four non-doped devices with a multilayer structure of ITO/ PEDOT: PSS (50 nm)/ NPB (60 nm)/ ADNs (40 nm)/ TPBI (20 nm)/ LiF/ Al were fabricated. The OCADN based device showed a reasonable good performance among these four studied blue devices, with maximum brightness of 5839 cd/m^2, current efficiency of 2.25 cd/A, power efficiency of 1.13 lm/W and a sky-blue color purity of CIE (0.16, 0.30).

Results and discussion

Synthesis and characterization

The synthetic routes of the intermediates and target compounds were shown in **Scheme. 1** and **2**. The starting materials 1-2 and 2-bromo-9,10-di(naphthalen-2-yl)anthracene were obtained from Shanghai Taoe chemical technology Co., Ltd. Other intermediates 3-6 were synthesized according to literature with

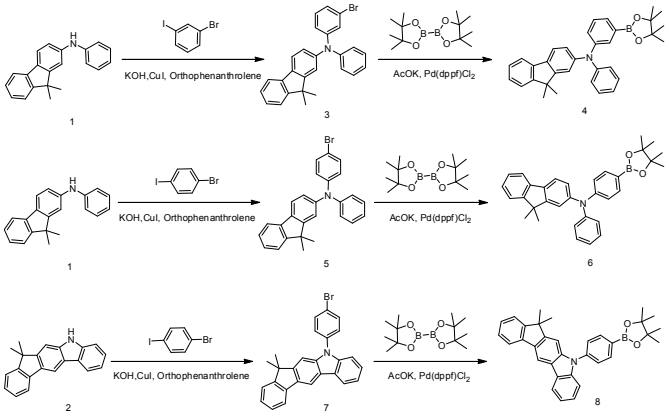

Scheme. 1 Synthetic routes of intermediates 3-8.

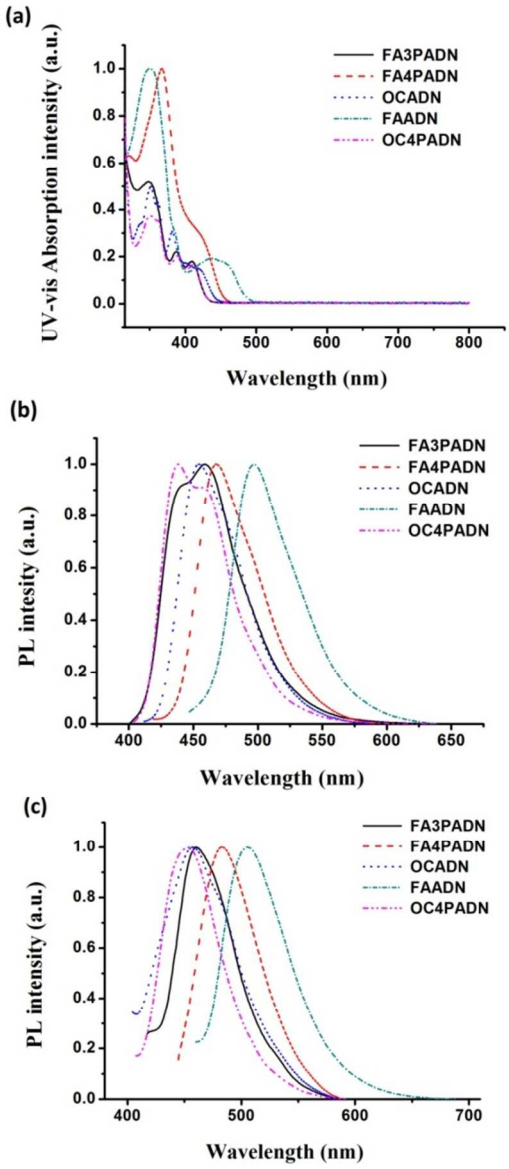

Fig. 1 (a) UV-Vis absorption spectra of all ADN derivatives in toluene. (b) PL spectra of all ADN derivatives in toluene and (c) PL spectra of these compounds in thin film.

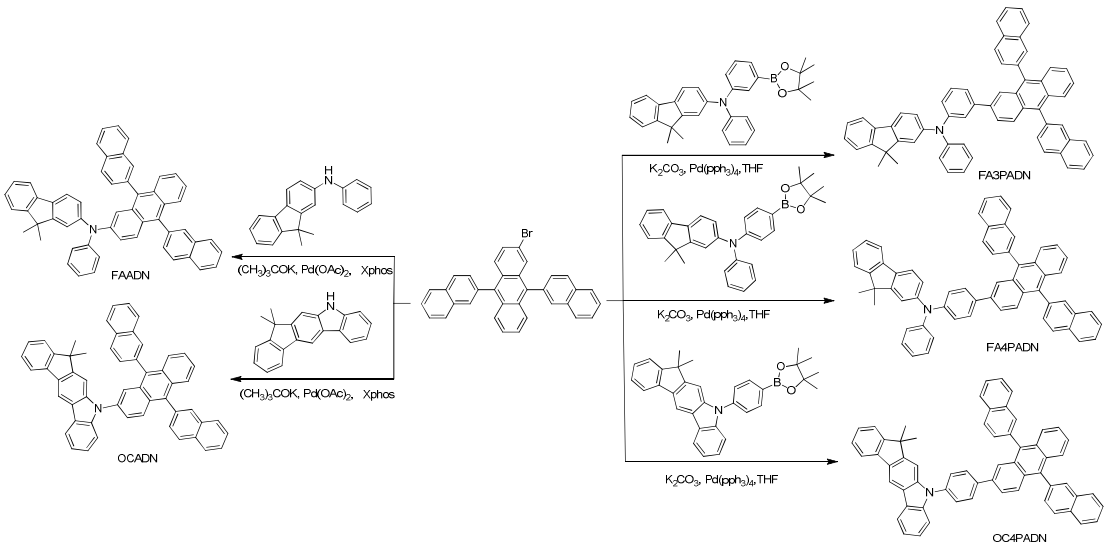

Scheme. 2 Synthetic routes of **ADN** derivatives.

high yields.[46-48] The target products were prepared by Buchwald-Hartwig and Suzuki coupling reaction between the 2-bromo-9,10-di(naphthalen-2-yl)anthracene and the corresponding aryl amine or aryl boronic acid, then purified by flash column chromatograph and recrystallization with yields of 32-62.5%. Repeated temperature-gradient vacuum sublimation was required for further purification of these ADN derivatives when used in OLEDs. The molecule structures of these compounds were characterized by ^{1}H NMR, ^{13}C NMR spectroscopy, and high-resolution mass spectrometry (HRMS).

Photophysical properties

The absorption and emission spectra of ADN derivatives were studied in toluene and solid thin films, which were dissolved in dichloromethane solution with PMMA and spin-coating on quartz plates. As shown from spectra, the UV-Vis absorption spectrum of ADN derivatives exhibits characteristic peaks in the range from 350 to 460 nm, which is attributed to the π-π* transition of the characteristic vibrational structures of anthracene groups. **FA4PADN** and **FAADN** showed broadening and red-shifting of the absorption spectra compared with other three compounds due to the stronger electron donating ability of fluorenamine moiety and their larger π-electron conjugation of molecule.

As shown in **Fig. 1**, all the compounds exhibited the maximum emission wavelength at around 438-497 nm in toluene and 453-505 nm in the solid thin film. The slight red shifted in the emission spectrum of the thin film from the solution could be attributed to the intermolecular π-π stacking of these ADN derivatives. All of these derivatives exhibited blue fluorescent color both in toluene and in solid state. It indicated that the co-planarity and π conjugation of molecule have been disrupted to some extent by the twist between functionalized moieties and anthracene core. **OCADN** and **OC4PADN**, which modified by indenocarbazole, showed blue-

Table. 1 Optical and thermal properties of ADN derivatives

ADN derivatives	λ_{ab}[a] (nm)	$\lambda_{set\ on}$[a] (nm)	λ_{fl}[a] (nm)	Φ_f[a] (%)	λ_{fl}[b] (nm)	HOMO[c] (eV)	LUMO[c] (eV)	E_g[d] (eV)	T_d[e](°C)
FA3PADN	410	431	459	38	460	-5.17	-2.29	2.88	423
FA4PADN	426	453	468	62	483	-5.10	-2.36	2.73	495
OCADN	423	445	454	46	458	-5.34	-2.55	2.79	408
FAADN	458	489	497	64	505	-5.02	-2.48	2.53	407
OC4PADN	412	431	438	46	453	-5.35	-2.47	2.88	492

[a]Measured in toluene. [b]Measured in thin film on quartz substrate. [c]Measured versus ferrocene, The HOMO and LUMO energy levels were determined using the following equations: $E_{HOMO} = [E_{ox} - E_{1/2}(\text{ferrocene}) + 4.8]$, $E_{LUMO} = E_{HOMO} - E_g$. [d]Obtained from onset of the absorption spectra by extrapolation ($E_g = 1240/\lambda_{set\ on}$). [e]Measured by TGA at a heating rate of 10 °C min^{-1}.

shifting of the emission peaks compared to other three compounds. It implied that the more rigid and planar conformation of indenocarbazole effectively increased the steric hindrance and interrupted the π conjugation between the substituted unit and ADN core. However, the compounds with the same substituted group (**FAADN** and **FA4PADN** or **OCADN** and **OC4PADN**) exhibited totally different maximum emission peak in the similar order (**FA4PADN**<**FAADN** or **OC4PADN** <**OCADN**). It showed that the incorporation of phenyl ring significantly increased the molecule twist and reduced the π conjugation. In addition, the maximum emission of the para-disposition linkage compound (**FA4PADN**) was observed at long wavelength with respect to that of the meta-disposition isomer (**FA3PADN**), it would be attributed to the para-disposition linkage could partially enlarge the π conjugation between ADN core and fluorenamine group.

As shown in **Table. 1**, the fluorescence quantum yields of **OCADN**, **OC4PADN**, **FAADN**, **FA3PADN** and **FA4PADN** were measured from 33% to 64% in solution. The φ_f data were consistent with the PL emission, the φ_f of **FAADN** and **FA4PADN** were higher than **OCADN** and **OC4PADN** in toluene, which indicated that the fluorenamine unit enhanced the electron donating ability of the molecule.

Thermal property

The device lifetime of OLEDs is directly related to the thermal stability of the light-emitting layer. Thus, high thermal decomposition temperature (T_d) is desirable for a light-emitting material to be utilized in OLEDs. The thermal properties of ADN derivatives were investigated by thermogravimetry (TGA) measurement, the relative data are listed in **Table. 1** and are shown in **Fig. 2**. **OCADN**, **OC4PADN**, **FAADN**, **FA3PADN** and **FA4PADN**, which were C-2 modified ADN derivatives, exhibited high T_d (corresponding to 5% weight loss) of 408, 492, 407, 423, 495 °C, respectively. The values of T_d of **OC4PADN**, **FA3PADN** and **FA4PADN** are much higher than that of **OCADN** and **FAADN**, which is attributed to the presence of more aromatic rings in the molecule of **OC4PADN**, **FA3PADN** and **FA4PADN**. Due to the large-volume substituents at the C-2 position of ADN, all these five compounds revealed high thermal stability and were capable of enduring the vacuum thermal deposition process in OLED fabrication, which suggested that the emitting layer composed with these ADN derivates has stable morphological properties and was desirable for OLEDs with high stability and efficiency.[40,49]

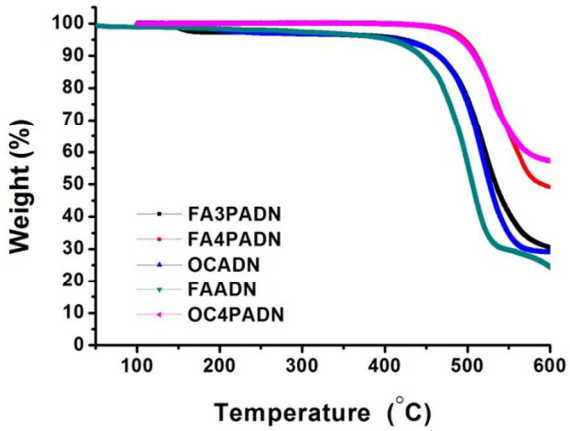

Fig. 2 TGA curves of all ADN derivatives.

Electrochemical properties

The electrochemical behavior of ADN derivatives was investigated by cyclic voltammetry using a standard three-electrode electrochemical cell in an electrolyte solution (0.1 M $TBAPF_6$/DCM), and ferrocene as external reference. The highest occupied molecular orbital (HOMO) estimated from the onset potentials of oxidation peak, were calculate to be -5.02 to -5.35 eV, while the lowest unoccupied molecular orbital (LUMO) of these derivatives measured by HOMO and band gap energy (E_g), were calculated to be -2.29 to -2.55 eV. The data of HOMO, LUMO energy levels and E_g was summarized in **Table 1**. The HOMO levels of **OCADN** and **OC4PADN** were lower than that of the other three compounds, which indicated that their greater steric hindrance between the ADN core and indenocarbazole moiety would dilute the electron density. In addition, the HOMO energy of these ADN derivatives were higher than those of ADN (-5.8 eV), due to the electron-donating functionalized moieties on C-2 position of ADN. It would certainly decrease the energy barrier between hole-transporting layer and light-emitting layer, and then further improve device performance.

Electroluminescence

In order to investigate the electroluminescence (EL) performance of these new blue emitting materials (excluding **FAADN**, which were spectroscopically unsatisfactory), four non-doped devices were fabricated by vacuum thermal deposition with the configuration of ITO/ PEDOT: PSS (50 nm)/ NPB (60 nm)/ ADNs (40 nm)/ TPBI (20 nm)/ LiF/ Al. Here, TIO was used as an anode electrode and the LiF/Al layers were employed as a composite cathode. Poly(3,4-ethylene dioxythiophene)/ poly(styrenesulfonate) (PEDOT: PSS) was used as the hole-injection layer, 4,4'-bis[N-(1-naphthyl)-N-phenyl-1-amino]-biphenyl (NPB) as the hole-transporting layer,

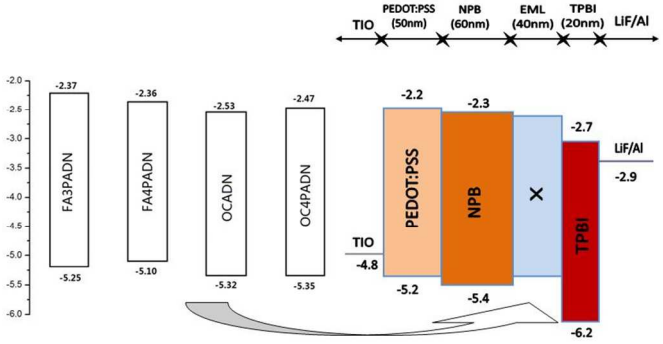

Fig. 3 Energy-level diagram of the materials used in devices.

Table. 2 Characteristics of OLEDs[a]

ADN derivatives	Turn-on Voltage[b] (V)	Max. luminance[c] (cd/m^2)	Max. efficiency[c] (cd/A, lm/W)	λ_{EL}, FWHM[d] (nm)	CIE(x,y)[e]
FA3PADN	4.5	4369	1.14, 0.65	487, 76	(0.18, 0.33)
FA4PADN	4.1	4490	1.43,0.85	486, 65	(0.17, 0.39)
OCADN	5.1	5839	2.25, 1.13	477, 62	(0.16, 0.30)
OC4PADN	5.6	3146	0.99, 0.48	451, 53	(0.16, 0.14)

[a]ITO/ PEDOT: PSS (50 nm)/ NPB (60 nm)/ ADNs (40 nm)/ TPBI (20 nm)/ LiF/ Al. [b]Turn-on voltage at 1 cd/m^2. [c]Maximum values. [d]Maximum EL emission peak and full-width-at-half-maximum were recorded at 8.0 V. [e]Commission Internationale d' Énclairage (CIE) at 6.0 V.

and 2,2',2''-(1,3,5-benzinetriyl)-tris(1-phenyl-1H-benzimidazole) (TPBI) as the electron-transporting layer and the hole-blocking layer. The structures and the energy levels of the materials used in these devices are demonstrated in **Fig. 3** and the key performance data were summarized in **Table. 2.**

The current density-voltage (*J*-V) curve of these four devices is displayed in **Fig. 4 (a)**. As we can see, the turn-on voltages were range from 4.1 to 5.6 eV. The primary reason for the low turn-on voltage is that the HOMO and LUMO energy level of ADN derivatives are matched with the NPB and TPBI, which reduced the energy barrier between hole/electron transporting layer and emitting layer, and then profited the hole and electron transporting and recombination in emitting layer. **Fig. 4 (b)** depicted the luminance versus voltage (L-V) of the devices. The device which used OCADN as emitting material showed a maximum brightness of 5839 cd/m^2 at 10 V, **FA3PADN**, **FA4PADN** and **OC4PADN** have maximum luminance 4369, 4490 and 3146 cd/m^2, respectively. **Fig. 5 (a)** and **(b)** presented

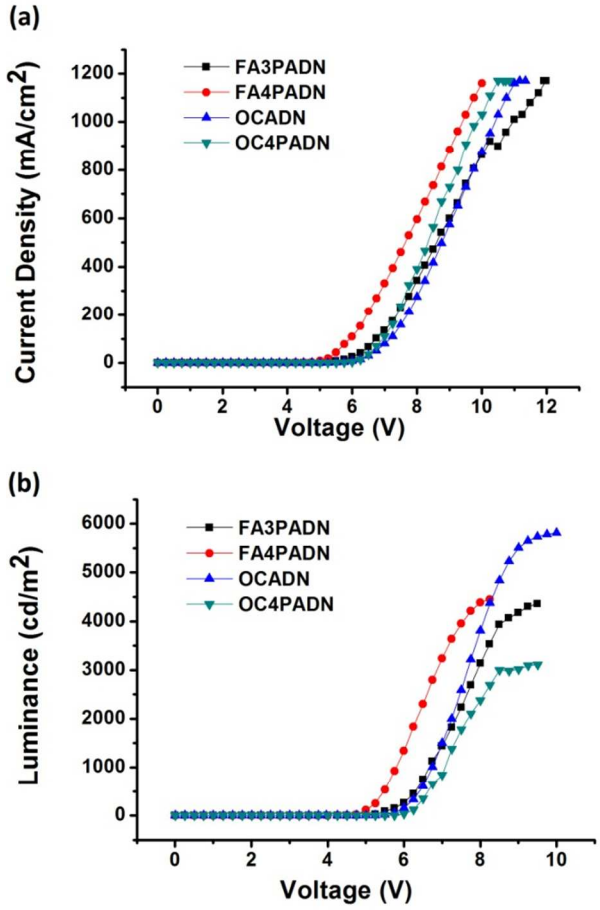

Fig. 4 (a) Current density-voltage characteristics and (b) Luminance-voltage characteristics of the four devices.

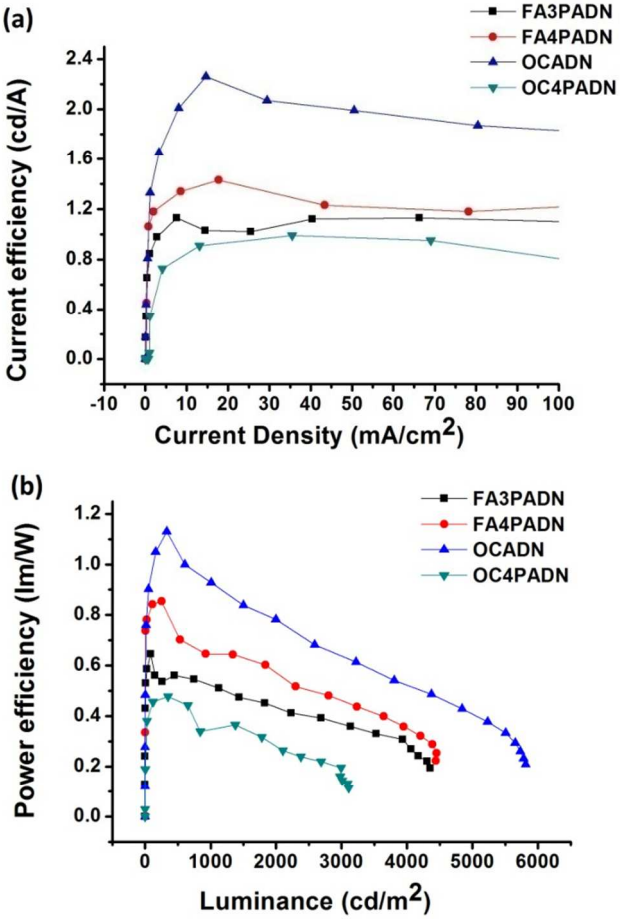

Fig. 5 (a) Current efficiency and (b) Power efficiency of the four device.

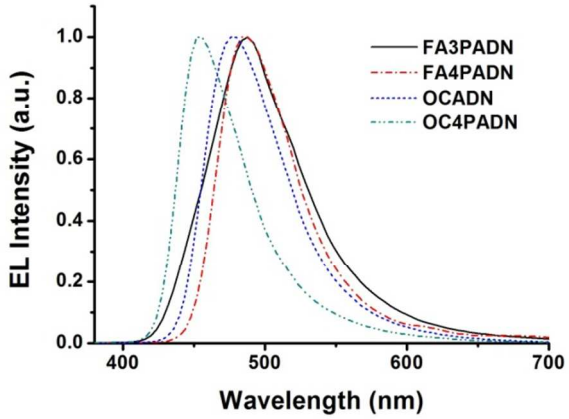

Fig. 6 EL spectra of the four devices.

the current efficiency (IE) and luminousefficiency (LE) of the fabricated devices. Among the four devices, the **OCADN** based device exhibited most efficient performance with current efficiency of 2.25 cd/A with power efficiency of 1.13 lm/W, it mainly attributed to its lowest LUMO energy level and the smallest energy barrier between OCADN and TPBI among these four compounds, which was helpful for electron transporting. Meanwhile, its relative lower HOMO energy level was also reduced the barrier between hole-transporting layer and emitting layer and beneficial for hole transporting. The devices with these four materials, especially the OCADN, showed high maximum brightness, maximum current and power efficiency. It indicated that the incorporation of florenamine or indenocarbazole moiety was helpful for improve the device performance. And it was worthwhile to note that all four devices showed a near flat current efficiency versus current density response, which indicated that the hole transporting nature of indenocarbazole and fluorenamine unit could reduce the efficiency roll-off and enhance the EL performance of device.

From the EL spectra shown in **Fig. 6**, we can know that all of these devices exhibited blue emissions with maximum emission peaks at 486, 487, 477, 451 nm and the corresponding CIE coordinates of devices were (0.18, 0.33), (0.17, 0.39), (0.16, 0.30) and (0.16, 0.14) at 8.0 V, respectively. The devices with our four materials maintained good EL emission in the blue region spectrum, which suggested that the red shifting were effectively suppressed when these materials used as emitter to devices. In accordance with the solid state PL emission, the device of **OC4PADN** and **OCADN** exhibited deeper blue EL compared with **FA3PADN** and **FA4PADN**. It could be attributed to the larger steric hindrance between the rigid and co-planar indenocarbazole unit and the ADN core, which reduced the coplanarity and π conjugation between the two moieties. Moreover, the device using **OC4PADN** as emitter showed the most deep-blue emission with the $CIE_{(x,y)}$ of (0.16, 0.14) at 8.0 V, due to the more twisty configuration of **OC4PADN** which incorporation a phenyl ring between the donor and the anthracene core. Furthermore, it was worthing to note that there is almost no EL color shift vary different driving voltages for all devices, it demonstrated that the hole-electron pairs for recombination were well confined in the blue emitter layer. The EL spectra of these four devices under different driving voltages were shown in the (ESI†).

Experimental

Materials

All starting materials were purchased from J & K Chemical Co., Aladdin Chemical Co. and Shanghai Taoe chemical technology Co., Ltd. without further purification. Solutions were carefully dried and distilled from appropriate drying agents prior to use. All reactions and manipulations were carried out under N_2 atmosphere. Silica gel (300-400 mesh) column chromatography was used as the stationary phase in the column.

The ^1H NMR and ^{13}C NMR spectra were measured using a Bruker AM 400 spectrometer. The mass spectra were obtained on a Waters LCT Premier XE spectrometer. The ultraviolet–visible (UV-Vis) absorption spectra of the samples were characterized using a Varian Cary 500 spectrophotometer. Photolumine-scence (PL) measurements were conducted by a Varian-Cary fluorescence spectrophotometer at room temperature. The cyclic voltammetry experiments were performed by a Versastat II electrochemical workstation (Princeton applied research) using a conventional three-electrode configuration with a glassy carbon working electrode, a Pt wire counter electrode, and a regular calomel reference electrode in saturated KCl solution, 0.1 M tetrabutylammonium hexafluorophosphate ($TBAPF_6$) in dichloromethane solution as the supporting electrolyte with a scan rate of 100 mV/s. The $E_{1/2}$ values were determined by $(E_{pa} + E_{pc})/2$ using Ferrocene as an external standard, where E_{pa} and E_{pc} were the anodic and catholic peak potentials, respectively. Thermo gravimetric analysis was carried out using a TGA instrument under a nitrogen atmosphere with a heating scan rate of 10 °C/min.

Synthesis

The synthesis of intermediates and ADN derivatives (**FAADN**, **OCADN**, **FA3PADN**, **FA4PADN**, **OC4PADN**) are presented in **Schemes. 1 and 2.**

Synthesis of 2-((3-bromophenyl)(phenyl)methyl)-9,9-dimethyl-9H-fluorene (3).

A mixture of 1-bromo-3-iodobenzene(4.23 g, 0.015 mol), 9,9-dimethyl-N-phenyl-9H-fluoren-2-amine (2.85 g, 0.01 mol), potassium hydroxide (2.81 g, 0.05 mol), cuprous iodide (0.095 g, 0.5 mmol) and orthophenanthrolene (0.09 g, 0.5 mmol) in 1,3,5-trimethylbenzene (80 ml) was stirred at 170 °C for 8 h under nitrogen atmosphere. After cooling to room temperature, the solution was evaporated to dryness under reduced pressure. The cold water was then added to the mixture and finally extracted with DCM. The combined organic phase was collected, filtered and dried over $MgSO_4$. The subjection of the crude mixture to silica gel chromatography using petroleum

ether/ dichloromethane (4:1, v/v) afforded 3 (2.43 g, yield: 55.4 %) as milky white solid. ^{1}H NMR (400 MHz, DMSO) δ 7.77 (m, *J* = 10.6, 7.4 Hz, 2H), 7.52 (d, *J* = 6.8 Hz, 1H), 7.39-7.34 (m, 2H), 7.34-7.26 (m, 3H), 7.22 (t, *J* = 8.0 Hz, 1H), 7.17-7.08 (m, 4H), 7.06-6.99 (m, 2H), 6.97-6.92 (m, 1H), 1.37 (d, *J* = 7.2 Hz, 6H).

Synthesis of 9,9-dimethyl-N-phenyl-N-(3-(4,4,5,5-tetramethyl-1,3,2-dioxabo- rolan-2-yl)phenyl)-9H- fluoren-2- amine (4).

50 ml of anhydrous 1,4-dioxane was added to a mixture of 3 (1.09 g, 2.5 mmol), bis(pinacolato) diboron(0.95 g, 3.75 mmol), potassium acetate (0.74 g, 7.5 mmol), [1,1'-Bis(diphenyl-phosphino) ferrocene]palladium(II) dichloride ($Pd(dppf)Cl_2$) (Catalytic amount). The reaction mixture was stirred at 100 °C for 2 h under nitrogen atmosphere. After the reaction was worked up by adding water, the organic layer was extracted with DCM and solution was evaporated. The crude product was purified by column chromatography using petroleum ether/ dichloromethane (5:1 v/v) as eluent. Afforded 4 (0.88 g, yield: 72.0 %) as white solid. ^{1}H NMR (400 MHz, DMSO) δ 7.72 (d, *J* = 8.2 Hz, 2H), 7.50 (d, *J* = 7.2 Hz, 1H), 7.39-7.29 (m, 6H), 7.29-7.24 (m, 1H), 7.20 (d, *J* = 2.0 Hz, 1H), 7.14 (m, 1H), 7.06 (m, 3H), 6.91 (m, 1H), 1.35 (s, 6H), 1.24 (s, 12H).

Synthesis of 2-((4-bromophenyl)(phenyl)methyl)-9,9-dimethyl-9H-fluorene (5).

Compound 5 (2.15 g, yield: 49.0 %) was synthesized as a white solid in a similar manner of 3 with 1-bromo-4-iodobenzene instead of 1-bromo-3-iodobenzene. ^{1}H NMR (400 MHz, DMSO) δ 7.74 (m, 2H), 7.51 (d, *J* = 6.8 Hz, 1H), 7.46-7.40 (m, 2H), 7.36-7.29 (m, 3H), 7.28 (m, 1H), 7.24 (m, 1H), 7.11-7.03 (m, 3H), 6.97 (m, 1H), 6.95-6.89 (m, 2H), 1.36 (s, 6H).

Synthesis of 9,9-dimethyl-N-phenyl-N-(4-(4,4,5,5-tetramethyl-1,3,2-dioxabor- olan-2-yl)phenyl)-9H- fluoren-2-amine (6).

Compound 6 (1.07 g, yield: 87.7 %) was synthesized as a white solid in a similar manner of 4 with 5 instead of 3. ^{1}H NMR (400 MHz, $CDCl_3$) δ 7.70-7.65 (m, 2H), 7.65-7.62 (m, 1H), 7.58 (d, *J* = 8.2 Hz, 1H), 7.41-7.37 (m, 1H), 7.29 (m, 3H), 7.25-7.19 (m, 2H), 7.15 (m, 2H), 7.12-7.05 (m, 3H), 7.03 (m, 1H), 1.41 (s, 6H), 1.34 (s, 12H).

Synthesis of 5-(4-bromophenyl)-7,7-dimethyl-5,7-dihydroindeno [2,1b] carbazole (7).

Compound 7 (2.78 g, yield: 63.7 %) was synthesized as a white solid in a similar manner of 3 with 2 instead of 1. ^{1}H NMR (400 MHz, $CDCl_3$) δ 8.43 (d, *J* = 0.6 Hz, 1H), 8.19 (d, *J* = 7.8 Hz, 1H), 7.85 (d, *J* = 7.4 Hz, 1H), 7.81-7.73 (m, 2H), 7.54-7.46 (m, 2H), 7.45-7.26 (m, 7H), 1.51 (s, 6H).

Synthesis of 7,7-dimethyl-5-(4-(4,4,5,5-tetramethyl-1,3,2-dioxa-borolan-2-yl) phenyl)-5,7-dihydroindeno [2,1-b] carbazole (8).

Compound 8 (0.85 g, yield: 70.2 %) was synthesized as a white solid in a similar manner of 4 with 7 instead of 3. ^{1}H NMR (400 MHz, $CDCl_3$) δ 8.43 (s, 1H), 8.19 (d, *J* = 7.8 Hz, 1H), 8.10 (d, *J* = 8.0 Hz, 2H), 7.84 (t, *J* = 8.6 Hz, 1H), 7.63 (t, *J* = 8.8 Hz, 2H), 7.40 (m, 5H), 7.29 (q, *J* = 6.8 Hz, 2H), 1.50 (s, 6H), 1.41 (s, 12H).

Synthesis of N-(9,9-dimethyl-9H-fluoren-2-yl)-9,10-di(naphtha-len-2-yl)-N-phenylanthracen-2-amine (FAADN).

A mixture of 9,9-dimethyl-N-phenyl-9H-fluoren-2-amine (0.3 g, 1.05 mmol), 2-bromo-9,10-di-(naphthalen-2-yl)anthracene (0.53 g, 1.05 mmol), potassium tert-butoxide (0.14 g, 1.26 mmol), palladium acetate (0.01 g, 0.05 mmol) and 2-dicyclohexyl phosphino-2',4',6'-triisopropylbi-phenyl (Xphos, 0.036 g, 0.11 mmol) was dissolved in 1,3,5-trimethylbenzene (30 mL) and heated at 170 °C for 8 h under nitrogen. After cooling, the solution removed under reduced pressure. Then the water was poured into the mixture and extracted with DCM. The organic layer was collected, filtered and dried by $MgSO_4$, the crude product was further purified by column chromatography using petroleum ether/dichloromethane (4:1, v/v). Finally afforded **FAADN** (0.32 g, yield: 42.6 %) as yellow solid. ^{1}H NMR (400 MHz, DMSO) δ 8.20 (d, *J* = 8.4 Hz, 1H), 8.14-8.04 (m, 3H), 7.90-7.77 (m, 4H), 7.73 (d, *J* = 7.2 Hz, 1H), 7.70-7.61 (m, 4H), 7.59-7.51 (m, 3H), 7.48-7.40 (m, 3H), 7.38-7.13 (m, 9H), 7.10 (s, 1H), 7.03 (d, *J* = 7.6 Hz, 2H), 6.95 (m, 2H), 1.17 (d, *J* = 15.8 Hz, 6H). ^{13}C NMR (101 MHz, $CDCl_3$) δ 153.58, 147.21, 146.71, 144.75, 138.98, 136.90, 136.02, 134.93, 133.41, 132.76, 132.43, 131.00, 130.21, 129.54, 129.06, 128.11, 127.60, 126.68, 126.23, 125.30, 124.41, 123.77, 122.45, 120.61, 119.49, 119.08, 117.71, 46.71, 26.94, 26.87. HRMS (ESI, *m/z*): $[M+H]^+$ calcd for $C_{55}H_{40}N$, 714.3161, found 714.3167.

Synthesis of 5-(9,10-di(naphthalen-2-yl)anthracen-2-yl)-7,7-di-methyl-5,7-dihydroindeno[2,1-b]carbazole (OCADN).

OCADN (0.17 g, yield: 54.0 %) was synthesized as a yellow solid in a similar manner of **FAADN** with 2 instead of 1. ^{1}H NMR (400 MHz, $CDCl_3$) δ 8.33 (d, *J* = 8.0 Hz, 1H), 8.19-7.96 (m, 9H), 7.91-7.84 (m, 2H), 7.84-7.58 (m, 8H), 7.49 (m, 3H), 7.43-7.29 (m, 6H), 7.28-7.26 (m, 1H), 7.23 (d, *J* = 7.0 Hz, 1H), 1.57 (s, 6H). ^{13}C NMR (101 MHz, $CDCl_3$) δ 153.38, 141.27, 139.94, 137.52, 137.01, 136.59, 133.53, 132.90, 132.36, 130.73, 130.22, 129.66, 128.79, 128.25, 127.99, 127.12, 126.58, 125.62, 125.01, 124.65, 123.62, 122.96, 122.53, 120.08, 119.34, 111.29, 109.91, 103.99, 53.46, 46.80, 27.98. HRMS (ESI, *m/z*): $[M+H]^+$ calcd for $C_{55}H_{38}N$, 712.3004, found 712.3000.

Synthesis of N-(3-(9,10-di(naphthalen-2-yl)anthracen-2-yl) phenyl)-9,9-dimethyl-N-phenyl-9H-fluoren-2-amine (FA3PADN).

2-bromo-9,10-di(naphthalen-2-yl)anthracene (0.38 g, 0.75 mmol), 4 (0.25 g, 0.5 mmol), 2M aqueous potassium carbonate (10 mL) was added to the 20 mL anhydrous tetrahydrofuran. After tetrakis(triphenylphosphine)palladium(0) ($Pd(PPh_3)_4$) (Catalytic amount) was added to the mixture, it was stirred under reflux for 4 h under nitrogen atmosphere. The reaction mixture was poured into water, and the aqueous solution was extracted with DCM. The extracts were washed with water and dried over magnesium sulfate. After the solution was evaporated, the crude product was purified by silica gel chromatography using petroleum ether/dichloromethane (4:1, v/v). Afforded **FA3PADN** (0.25 g, yield: 62.5 %) as yellow solid. ^{1}H NMR (400 MHz, $CDCl_3$) δ 8.10-7.87 (m, 6H), 7.83 (m, 3H), 7.71-7.59 (m, 3H), 7.59-7.47 (m, 7H), 7.44 (d, *J* = 8.2 Hz, 1H), 7.38 (m, 1H), 7.29 (d, *J* = 7.2 Hz, 1H), 7.25-7.19 (m, 4H), 7.18-7.13 (m, 1H), 7.10 (m, 2H), 7.07-6.96 (m, 5H), 6.92 (m, 2H), 6.84

(m, 1H), 1.29 (t, J = 5.1 Hz, 6H). ^{13}C NMR (101 MHz, $CDCl_3$) δ 152.51, 147.37, 145.99, 141.01, 137.92, 136.33, 132.42, 131.78, 129.26, 128.47, 128.10, 127.01, 126.06, 125.90, 125.43, 125.22, 124.19, 123.37, 123.14, 122.56, 121.77, 121.43, 121.22, 120.20, 119.56, 118.42, 117.91, 45.75, 26.01. HRMS (ESI, *m/z*): $[M+H]^+$ calcd for $C_{55}H_{38}N$, 790.3474, found 790.3470.

Synthesis of 9,9-dimethyl-N-phenyl-N-(4-(4,4,5,5-tetramethyl-1, 3,2-dioxaborolan-2-yl)phenyl)-9H-fluoren-2-amine (FA4PADN). **FA4PADN** (0.17 g, yield: 54.0 %) was synthesized as a yellow solid in a similar manner of **FA3PADN** with 6 instead of 4. ^{1}H NMR (400 MHz, $CDCl_3$) δ 8.10 (m, 2H), 8.07-7.99 (m, 4H), 7.98-7.89 (m, 3H), 7.81 (d, J = 9.2 Hz, 1H), 7.77-7.70 (m, 2H), 7.69-7.64 (m, 2H), 7.60 (m, 6H), 7.55 (d, J = 8.2 Hz, 1H), 7.38 (t, J = 8.0 Hz, 3H), 7.32-7.27 (m, 3H), 7.22 (d, J = 7.4 Hz, 3H), 7.17 (d, J = 2.0 Hz, 1H), 7.11 (d, J = 7.6 Hz, 2H), 7.07 (d, J = 8.6 Hz, 2H), 7.01 (m, 2H), 1.38 (s, 6H). ^{13}C NMR (101 MHz, $CDCl_3$) δ 155.10, 147.67, 147.40, 138.92, 137.12, 136.60, 134.45, 133.49, 132.83, 130.56, 130.07, 129.67, 129.27, 127.92, 127.04, 126.96, 126.28, 125.27, 124.39, 123.75, 123.48, 122.92, 122.46, 120.64, 119.46, 119.01, 46.83, 27.07. HRMS (ESI, *m/z*): $[M+H]^+$ calcd for $C_{55}H_{38}N$, 790.3474, found 790.3476.

Synthesis of 7,7-dimethyl-5-(4-(4,4,5,5-tetramethyl-1,3,2-dioxa-borolan-2-yl)phenyl)-5,7-dihydroindeno carbazole (OC4PADN). **OC4PADN** (0.18 g, yield: 32.0 %) was synthesized as a white solid in a similar manner of **FA3PADN** with 8 instead of 4. ^{1}H NMR (400 MHz, $CDCl_3$) δ 8.42 (s, 1H), 8.16 (t, J = 8.4 Hz, 3H), 8.12-8.04 (m, 5H), 7.99 (d, J = 4.2 Hz, 2H), 7.92 (d, J = 9.2 Hz, 1H), 7.84 (d, J = 7.4 Hz, 1H), 7.81-7.68 (m, 7H), 7.65 (m, 4H), 7.59 (d, J = 8.6 Hz, 2H), 7.44-7.32 (m, 7H), 7.28 (m, 2H), 1.49 (s, 6H). ^{13}C NMR (101 MHz, $CDCl_3$) δ 155.02, 153.58, 147.21, 146.71, 144.75, 138.98, 136.90, 134.93, 134.72, 133.41, 133.12, 132.76, 132.43, 131.00, 130.49, 130.21, 129.06, 126.90, 126.23, 125.30, 123.77, 122.76, 122.45, 120.61, 119.49, 119.08, 117.71, 46.71. HRMS (ESI, *m/z*): $[M+H]^+$ calcd for $C_{55}H_{38}N$, 788.3317, found 788.3313.

Measurements and OLEDs fabrication

Organic layers were deposited on the indium-tin-oxide (ITO)/glass substrate by thermal evaporation. The ITO/glass substrate was cleaned sequentially by detergent, de-ionized water and ethanol. Then the ITO/glass was treated by oxygen (O_2) and polymerized fluorocarbon (CFx) plasma before loading into a 10-source evaporator, with a base pressure of 5.0×10^{-4} Pa, for device fabrication. All devices were encapsulated in a N_2 purged glove box connected to the evaporator after the fabricated for device characterization.

The current–voltage–luminance characteristics of the OLEDs were measured with a diode array rapid scan system using a Photo Research PR650 spectrophotometer and a computer-controlled, programmable, direct-current (DC) source. All measurements were carried out in ambient atmosphere at room temperature.

Conclusions

In summary, we have synthesized and characterized a series of ADN derivatives, **FAADN**, **OCADN**, **FA3PADN**, **FA4PADN** and **OC4PADN**. Expect for **FAADN**, the other four materials exhibited satisfactory blue fluorescence emission both in toluene and solid film, which attributed to the sterically hindered substituent at C-2 position of ADN. These compounds also showed excellent thermal properties and appropriate energy levels, which can be utilized as emitting materials for OLED device. As a result, a device base on **OCADN** with the structure of ITO/ PEDOT: PSS/ NPB/ ADNs/ TPBI/ LiF/ Al showed efficient blue emission peaked at 477 nm and CIE chromaticity coordinates of (0.16, 0.30). The maximum current efficiency and power efficiency of the device reached 2.25 cd/A and 1.13 lm/W, respectively.

Acknowledgements

Q. Dong thanks the financial support from the National Natural Science Foundation of China (Grant No.: 61307030), Program for the Outstanding Innovative Teams of Higher Learning Institutions of Shanxi (OIT), Fund Program for the Scientific Activities of Selected Returned Overseas Professionals in Shanxi Province, the Natural Science Foundation for Young Scientists of Shanxi Province, China (Grant No.: 2014021019-2), the Outstanding Young Scholars Cultivating Program, Research Project Supported by Shanxi Scholarship Council of China (Grant No.: 2014-02) and the Qualified Personal Foundation of Taiyuan University of Technology (Grant No.: 2013Y003, tyut-rc201275a).

References

1 J. H. Huang, J. H. Su and H. Tian, *J. Mater. Chem.*, 2012, **22**, 10977.
2 K. Walzer, B. Maennig, M. Pfeiffer, K. Leo, *Chem. Rev.*, 2007, **107**, 1233.
3 B. W. D'Andrade, S. R. Forrest, *Adv. Mater.*, 2004, **16**, 1585.
4 C. H. Yang, M. Mauro, F. Polo, S. Watanabe, I. Muenster, R. Fröhlich and L. D. Cola, *Chem. Mater.*, 2012, **24**, 3684.
5 Z. Z. Zheng, Q.C. Dong, L. Gou, J. H. Su, J. H Huang, *J. Mater. Chem.*, 2014, **2**, 9858.
6 C. W. Tang, S. A. VanSlyke, *Appl. Phys. Lett.*, 1987, **51**, 913.
7 Z. Y. Xia, Z. Y. Zhang, J. H. Su, Q. Zhang, K. M. Fung, M. K. Lam, K. F. Li, W. Y. Wong, K. W. Cheah, H. Tian, C. H. Chen, *J. Mater. Chem.*, 2010, **20**, 3768.
8 K. H Lee, J. K. Park, J. S. Park, J. H. Seo, Y. K. Kim, S. S. Yoon, *J. Mater. Chem.*, 2011, **21**, 13640.
9 J. H. Huang, J. H. Su, X. Li, M. K. Lam, K. M. Fung, H. H. Fan, K. W. Cheah, C. H. Chen, H. Tian, *J. Mater. Chem.*, 2011, **21**, 2957.
10 H. Fu, Y. M. Cheng, P. T. Chou, Y. Chi, *Mater. Today*, 2011, **14**, 472.
11 F. Kessler, Y. Watanabe, H. Sasabe, H. Katagirl, M. K. Nazeeruddin, M. Grätzel and J. Kido, *J. Mater. Chem*. C, 2013, **1**, 1070.
12 X. L. Yang, X. B. Xu, G.J. Zhou, *J. Mater. Chem*. C, 2015, **3**, 913.
13 H. Park, J. Lee, I. Kang, H. Y. Chu, J. I. Lee, S. K. Kwon, Y. H. Kim, *J. Mater. Chem.*, 2012, **22**, 2695.

14 Z. Q. Wang, C. Xu, W. Z. Wang, L. M. Duan, Z. Li, B.T. Zhao B.M. Ji, *New J. Chem.*, 2012, **36**, 662.
15 M. S. Gong, H. S. Lee and Y. M. Jeon, *J. Mater. Chem.*, 2012, **20**, 10735.
16 C. H. Wu, C. H. Chien, F. M. Hsu, P. I. Shih, C. F. Shu, *J. Mater. Chem.*, 2009, **19**, 1464.
17 S. L. Lai, Q. X. Tong, M. Y. Chan, T. W. Ng, M. F. Lo, S. T. Lee, C. S. Lee, *J. Mater. Chem.*, 2011, **21**, 1206.
18 T. M. Figueira-Duarte, P. G. D. Rosso, R. Trattnig, S. Sax, E. J. W. List, K. Mullen, *Adv. Mater.*, 2010, **22**, 990.
19 Y. C. Chang, S. C. Yeh, Y. H. Chen, C. T. Chen, R. H. Lee, R. J. Jeng, *Dyes Pigm.*, 2013, **99**, 577.
20 S. H. Kim, I. Cho, M. K. Sim, S. Park, S. Y. Park, *J. Mater. Chem.*, 2011, **21**, 9139.
21 L. Zhao, J. Zhou, J. Huang, C. Li, Y. Zhang, C. Sun, X. Zhu, J. Peng, Y. Cao, J. Roncali, *Org. Electron.*, 2008, **9**, 649.
22 Z. H. Zhang, W. Jiang, X. X. Ban, M. Yang, S. H. Ye, B. Huang, Y. M. Sun, *RSC Adv.*, 2015, **5**, 29708.
23 R. Kim, X. Q. Liu, S. G. Lee, J. H. Lee, Y. H. Kim, *Synth. Met.*, 2014, **197**, 68.
24 E. J. Na, K. H. Lee, B. Y. Kim, S. J. Lee, Y. K. Kim, S. S. Yoon, *Mol. Cryst. Liq. Cryst.*, 2015, **584**, 1072954.
25 S. J. Yoo, C. W. Jeon, J. J. Ha, S. Y. Nam, S. C. Shin, J. Hwang, Y. H. Kim, *Macromol. Res.*, 2013, **21**, 463.
26 J. W. Park, P. Kang, H. Park, H. Y. Oh, J. H. Yang, Y. H. Kim, S. K. Kwon, *Dyes Pigm.*, 2010, **85**, 93.
27 I. Kang, J. Y. Back, R. Kim, Y. H. Kim, S. K. Kwon, *Dyes Pigm.*, 2011, **92**, 588.
28 M. X. Yu, J. P. Duan, C. H. Lin, C. H. Cheng, Y. T. Tao, *Chem. Mater.*, 2002, **14**, 3958.
29 K. C. Wu, P. J. Ku, C. S. Lin, H. T. Shih, F. I. Wu, M. J. Huang, J. J. Lin, I. C. Chen, C. H. Cheng, *Adv. Funct. Mater.*, 2008, **18**, 67.
30 H. Y. Oh, C. Lee, S. Lee, *Org. Electron.*, 2009, **10**, 163.
31 H. Lee, B. Kim, S. Kim, J. Kim, J. Lee, H. Shin, J. H. Lee, J. Park, *J. Mater. Chem. C*, 2014, **2**, 4737.
32 M. G. Shin, S. O. Kim, H. T. Park, S. J. Park, H. S. Yu, Y. H. Kim, S. K. Kwon, *Dyes Pigm.*, 2012, **92**, 1075.
33 G. Y. Mu, S. Q. Zhuang, W. Z. Zhang, Y. X. Wang, B. Wang, L. Wang, X. J. Zhu, *Org. Electron.*, 2015, **21**, 9.
34 Y. Huang, X. Y. Du, S. Tao, X. X. Yang, C. J. Zheng, X. H. Zhang, C. S. Lee, *Synth. Met.*, 2015, **203**, 49.
35 G. Haykir, E. Tekin, T. Atalar, F. Türksoy, *Thin Solid Films*, 2013, **548**, 171.
36 J. Y. Song, S. B. Lee, S. J. Lee, Y. K. Kim, S. S. Yoon, *Thin Solid Films*, 2015, **577**, 42.
37 S. B. Lee, S. N. Park, C. Kim, H. W. Lee, H. W. Lee, Y. K. Kim, S. S. Yoon, *Synth. Met.*, 2015, **203**, 174.
38 J. Y. Song, S. N. Park, S. J. Lee, Y. K. Kim, S. S. Yoon, *Dyes Pigm.*, 2015, **114**, 40.
39 J. Shi and C. W. Tang, *Appl. Phys. Lett.*, 2002, **80**, 3201.
40 M. T. Lee, H. H. Chen, C. H. Liao, C. H. Tsai, C. H. Chen, *Appl. Phys. Lett.*, 2004, **85**, 3301.
41 M. T. Lee, H. H. Chen, C. H. Liao, C. H. Tsai, C. H. Chen, *Adv. Mater.*, 2005, **17**, 2493.
42 C. L. Wu, C. H. Chang, Y. T. Chang, C. T. Chen, C. T. Chen, C. J. Su, *J. Mater. Chem.*, 2014, **2**, 7188.
43 J. H. Kong, J. M. Lee, J. H. Kwon, J. K. Lee and J. H. Park, *RSC Adv.*, 2015, **5**, 31282
44 K. Danel, T. H. Huang, J. T. Lin, Y. T. Tao, and C. H Chuen, *Chem. Mater.*, 2002, **14**, 3860.
45 J. Y. Baek, Y. R. Cheon, H. G. Shin, J. W. Park, Y. H. Kim, *Optical Materials Express*, 2014, **4**, 1051.
46 S. O. Jeon, S. E. Jang, H. S. Son, J. Ye. Lee, *Adv. Mater.*, 2011, **23**, 1436.
47 S. J. Su, H. Sasabe, T. Takeda, J. Kido, *Chem. Mater.*, 2008, **20**, 1691.
48 H. Y. Chen, C. T. Chen, C. T. Chen, *Macromol.*, 2010, **43**, 3613.
49 J. H. Huang, B. X., M. K. Lam, K. W. Cheah, C. H. Chen, J. H. Su, *Dyes Pigm.*, 2011, **89**, 155.